Supporting Information

Emulating working memory consolidation with a 1D supramolecular nanofibre-based neuromorphic device

Tejaswini S. Rao[a], Subi J. George[b], Giridhar U. Kulkarni[a,]*

[a]Chemistry & Physics of Materials Unit, Jawaharlal Nehru Centre for Advanced Scientific Research, Jakkur P.O., Bangalore-560064, India

[b]Supramolecular Chemistry Laboratory, New Chemistry Unit, Jawaharlal Nehru Centre for Advanced Scientific Research, Bangalore-560064, India

** Corresponding Author & Email Address : Prof. Giridhar U. Kulkarni (kulkarni@jncasr.ac.in)*

Table S1. Comparison table demonstrating learning-forgetting-relearning imparted on the neuromorphic devices.

Sl.No	Active Material	Two/three -terminal	Stimuli	Number of relearning sessions held	Habituation/fatigue	Consolidation	Ref No
1	ZnO NPs	Two	Optical	1	×	×	1
2	HfO_x/BP	Two	Electrical/Optical	6	×	×	2
3	Graphene TiO_2	Two	Optical	3	×	×	3
4	P-$MoSe_2$/P_xO_y	Two	Electrical/optical	5	×	×	4
5	p-AlGaN/n-GaN/Pt NPs	Two	Optical	1	×	×	5
6	$CsPbIBr_2$	Two	Optical	1	×	×	6
7	a-Ga_2O_3	Two	Electrical/optical	2	×	×	7
8	Cu_2O/WO_3	Two	Electrical/optical	2	×	×	8
9	GeO_2 NP:PMMA	Two	Electrical	4	×	×	9
10	Al_2O_3/Al-HQ	Two	Electrical	1	×	×	10
11	Ag@TiO_2 NWN	Two	Electrical	1	×	×	11
12	C8-BTBT/PS/PAA	Three	Optical	1	×	×	12
13	a-ZnAlSnO	Three	Electrical/Optical	2/1	×	×	13
14	DNTT/MoS_2	Three	Optical	1	×	×	14
15	ITO-graphene	Three	Optical	2	×	×	15
16	MoS_2	Three	Optical	1	×	×	16
17	TiN/Li_xSiO_y/Pt	Two	Electrical	×	✓	×	17
18	Au/$LiTaO_3$/Pt	Two	Electrical	×	✓	×	18
19	TiO_{2-x}	Four	Electrical	×	✓	×	19

20	poly-Si/ SiO_2/Si_3N_4	Three	Electrical	×	✓	×	20
21	Pt/LLTO/Pt	Two	Electrical	×	✓	×	21
22	$W/HfO_x/Ti$	Two	Electrical	×	✓	×	22
23	ZnO Nanowire	Two	Electrical/optical	×	✓	×	23
24	$IGZO\text{-}HfO_2$	Two	Electrical	×	✓	×	24
25	TiO_x	Two	Electrical	×	✓	×	25
26	MSC-based electrolyte-gated MPEC ITO	Three	Electrical	×	✓	×	26
27	Supramolecular nanofibre	Two	Optical	32	✓	✓	This work

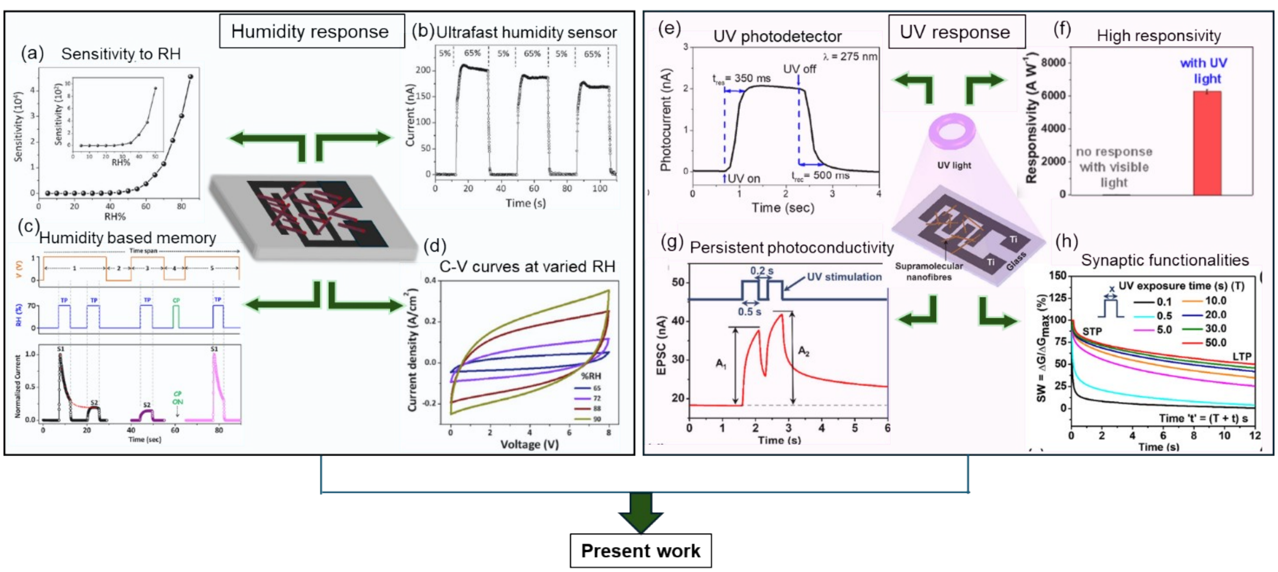

Figure S1 Previous reports on the remarkable humidity and UV sensitivity of the supramolecular nanofibre device. (a) Variation of sensitivity with RH. Reproduced with permission from Mogera et al., *Sci. Rep.*, 2014, **4**, 1–9.[27] Copyright 2014 Nature Portfolio. (b) Ultrafast humidity response. Reproduced with permission from Mogera et al., *Sci. Rep.*, 2014, **4**, 1–9.[27] Copyright 2014 Nature Portfolio. (c) Humidity-based memory behavior. Reproduced with permission from Mogera et al., *ACS Appl. Mater. Interfaces*, 2017, **9**, 32065–32070.[28] Copyright 2017 American Chemical Society. (d) C-V curves of the device with varied RH. Reproduced with permission from Kundu et al., *Nano Energy*, 2019, **61**, 259–266.[29] Copyright 2019 Elsevier. (e) Photoresponse of the device. Reproduced with permission from Kundu et al., *ACS Appl. Mater. Interfaces*, 2023, **15**, 19270–19278.[30] Copyright 2023 American Chemical Society. (f) High responsivity for UV light. Reproduced with permission from Kundu et al., *ACS Appl. Mater. Interfaces*, 2023, **15**, 19270–19278.[30] Copyright 2023 American Chemical Society. (g) Persistent photoconductivity exhibited under UV exposure. Reproduced with permission from Rao et al., *Nanoscale*, 2023, **15**, 7450–7459.[31] Copyright 2023 Royal Society of Chemistry.

(h) Emulation of synaptic functionalities based on the phenomenon of persistent photoconductivity. Reproduced with permission from Rao et al., *Nanoscale*, 2023, **15**, 7450–7459.[31] Copyright 2023 Royal Society of Chemistry.

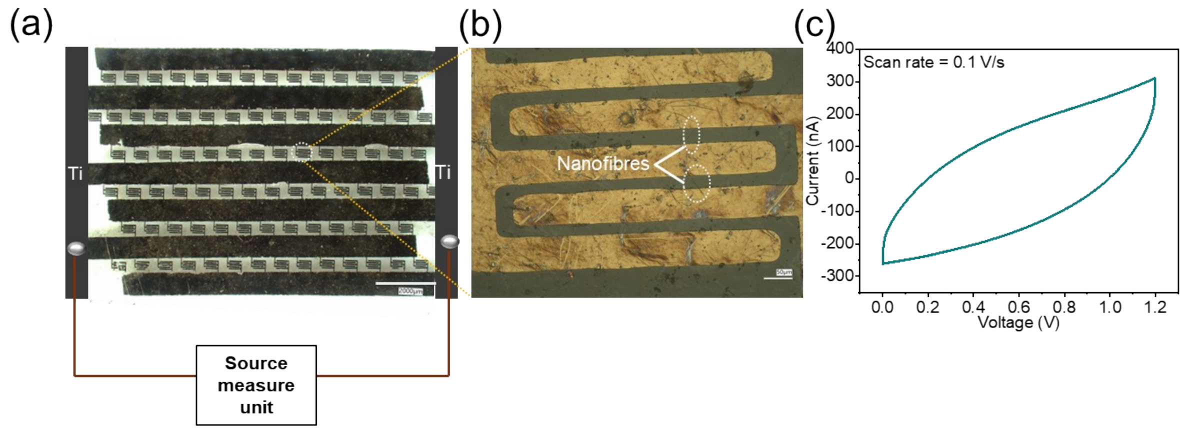

Figure S2 (a) Optical image of the entire device connected to a source measure unit. (b) Magnified optical image showing the nanofibres spread across the interdigitated electrodes. (c) I-V sweep from 0 to 1.2 V.

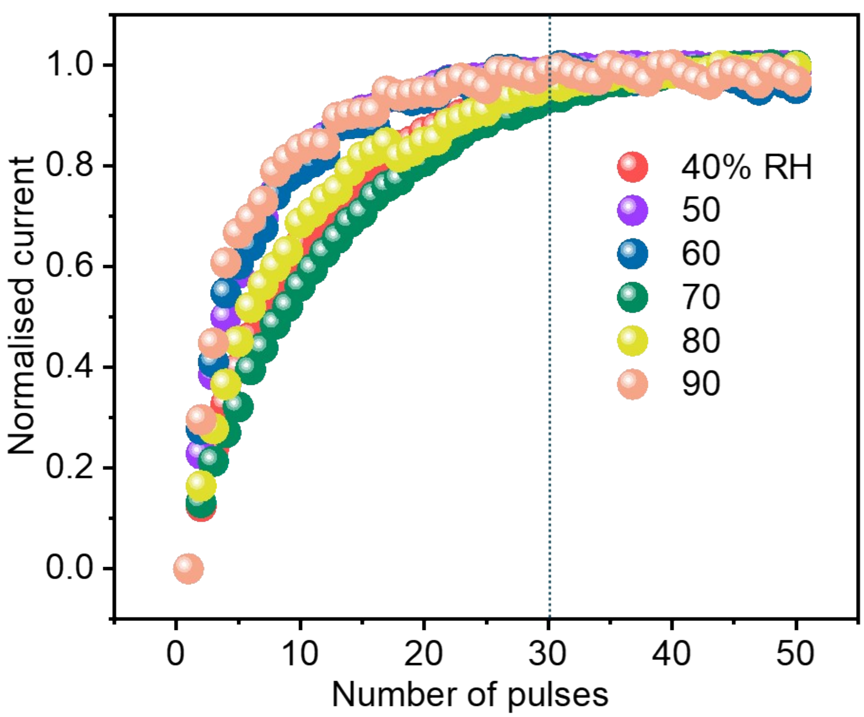

Figure S3 Normalized current response at different RH for 50 optical pulses exhibiting saturation around 30 pulses.

$$\% \ of \ current \ decay = \left(\frac{(A_1 - A_0) - (A_1' - A_0)}{A_1 - A_0}\right) \times 100$$

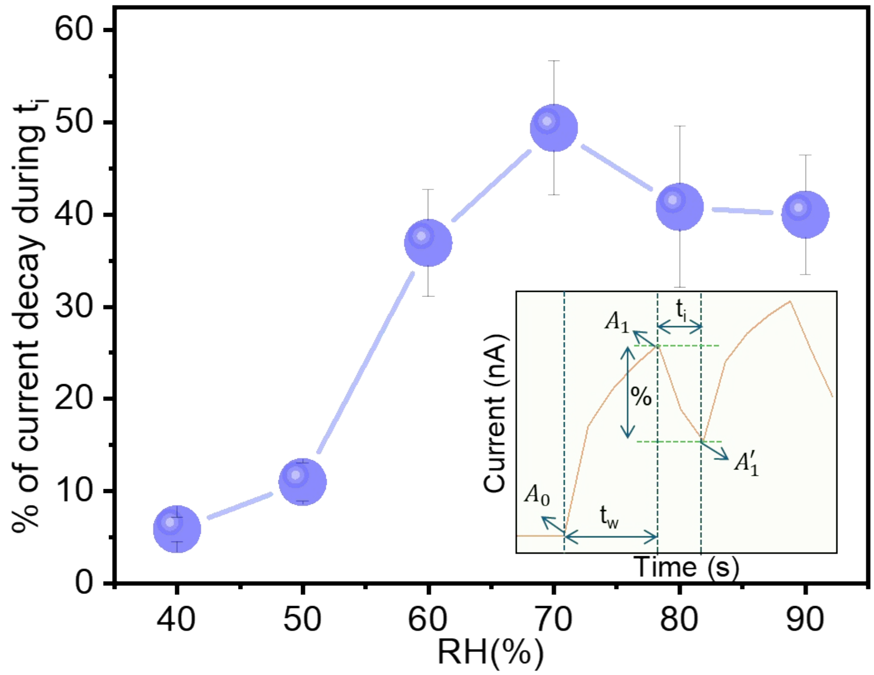

Figure S4 % of current decay during t_i (200 ms) between optical exposure at varied RHs. Inset shows the photoresponse for two optical pulses depicting the method of % decay calculation and the equation used is shown on the top.

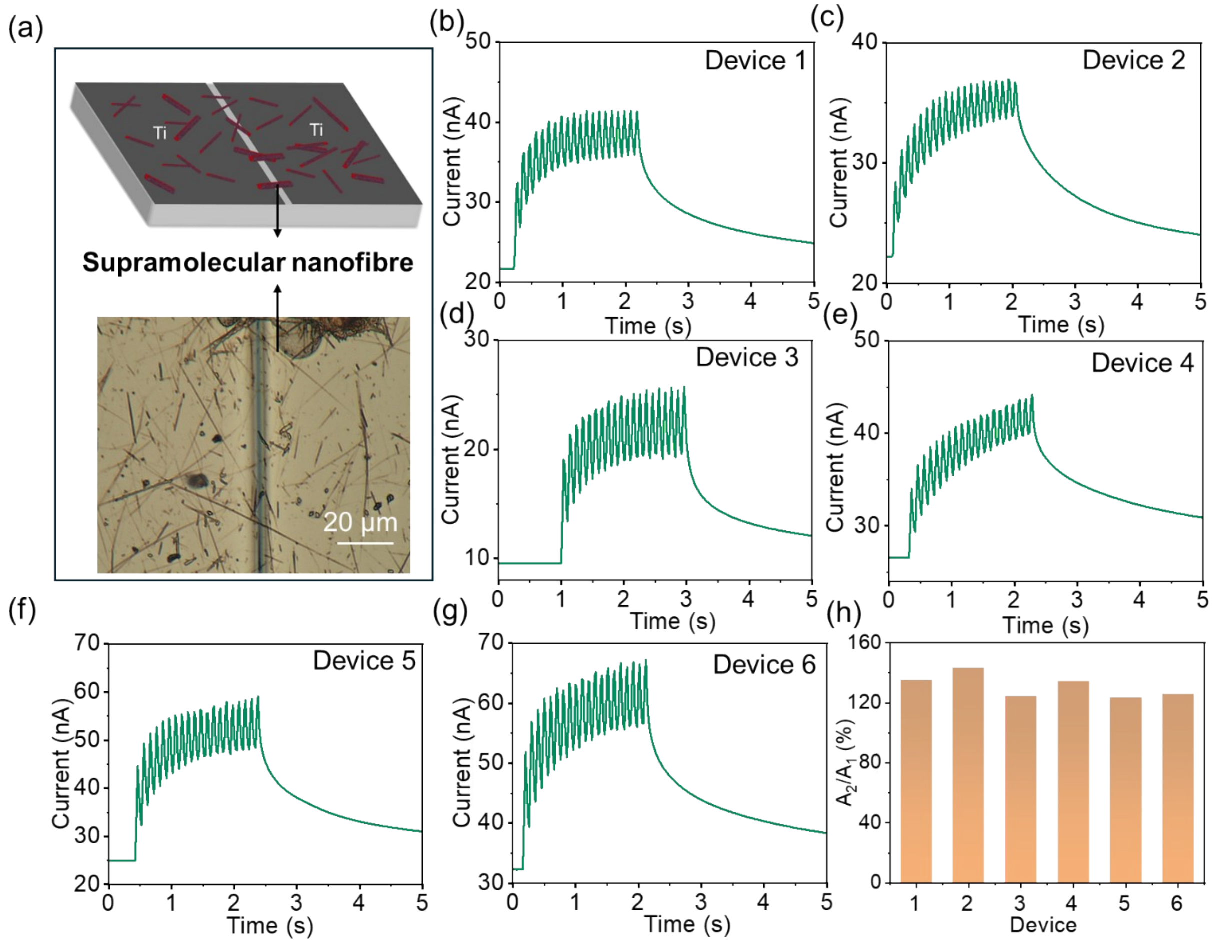

Figure S5 (a) Schematic of the device and the optical microscopy image of the nanofibres spread across the gap between Ti electrodes. (b-g) Six devices and their photoresponse studied at 70% RH. 20 optical pulses of 50 ms pulse width (t_w) and 50 ms pulse interval (t_i) are applied. (h) Paired pulse facilitation (PPF) index of all the six devices.

Note S1

The energy consumption of the device is calculated using the equation: $E = V \times I \times t$

Where V is the reading voltage, I is the peak current, and t is the pulse duration.

Substituting the values for $V = 1\ V$, I (for varied RH), and $t = 0.5\ s$, the energy consumption of the device per unit pulse of 0.5 s is found to be $E = 1 \times I \times 0.5 = \mathrm{x}\ nJ$ per pulse.

The energy consumption of x nJ per pulse is for the whole device with several nanofibres spread across the Ti electrodes. However, each nanofibre across the Ti electrodes acts as a synaptic junction.

On average, there are 15 nanofibres spread across the electrodes in a single IDT pattern. There are 85 IDT patterns, and therefore, the whole device consists of $85 \times 15 = 1275$ nanofibres.

Therefore, the power consumption per synaptic junction is given by;
x $nJ/1275$ = y pJ.

RH (%)	$I = (I_1\text{-}I_0)$ (nA)	Energy per optical pulse (x nJ)	Energy per synaptic junction (y pJ)
40	0.19	0.09	0.07
50	3.04	1.52	1.19
60	19.15	9.57	7.51
70	35.96	17.98	14.1
80	60.52	30.26	23.73
90	107.31	53.65	42.08

I_0 is the dark current and I_1 is the photocurrent achieved for the optical pulse

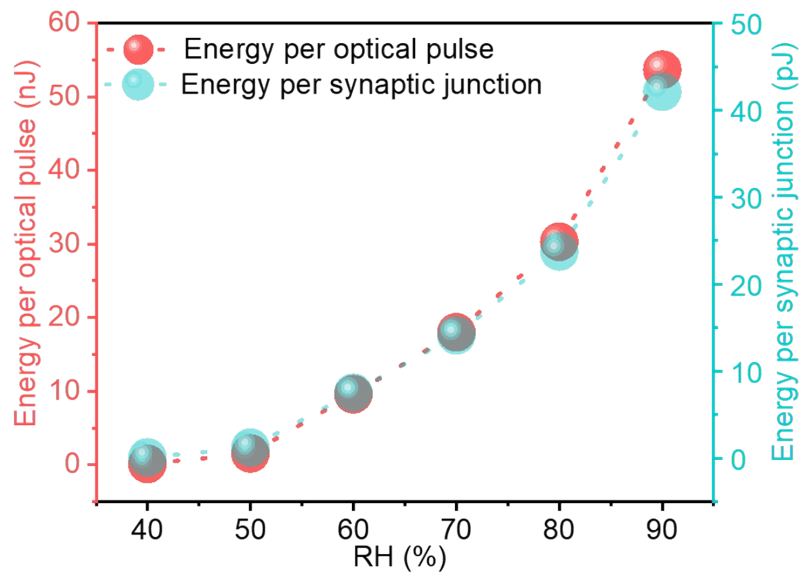

Figure S6 Energy consumption per optical pulse (red curve) and per synaptic junction (blue curve) at different RHs.

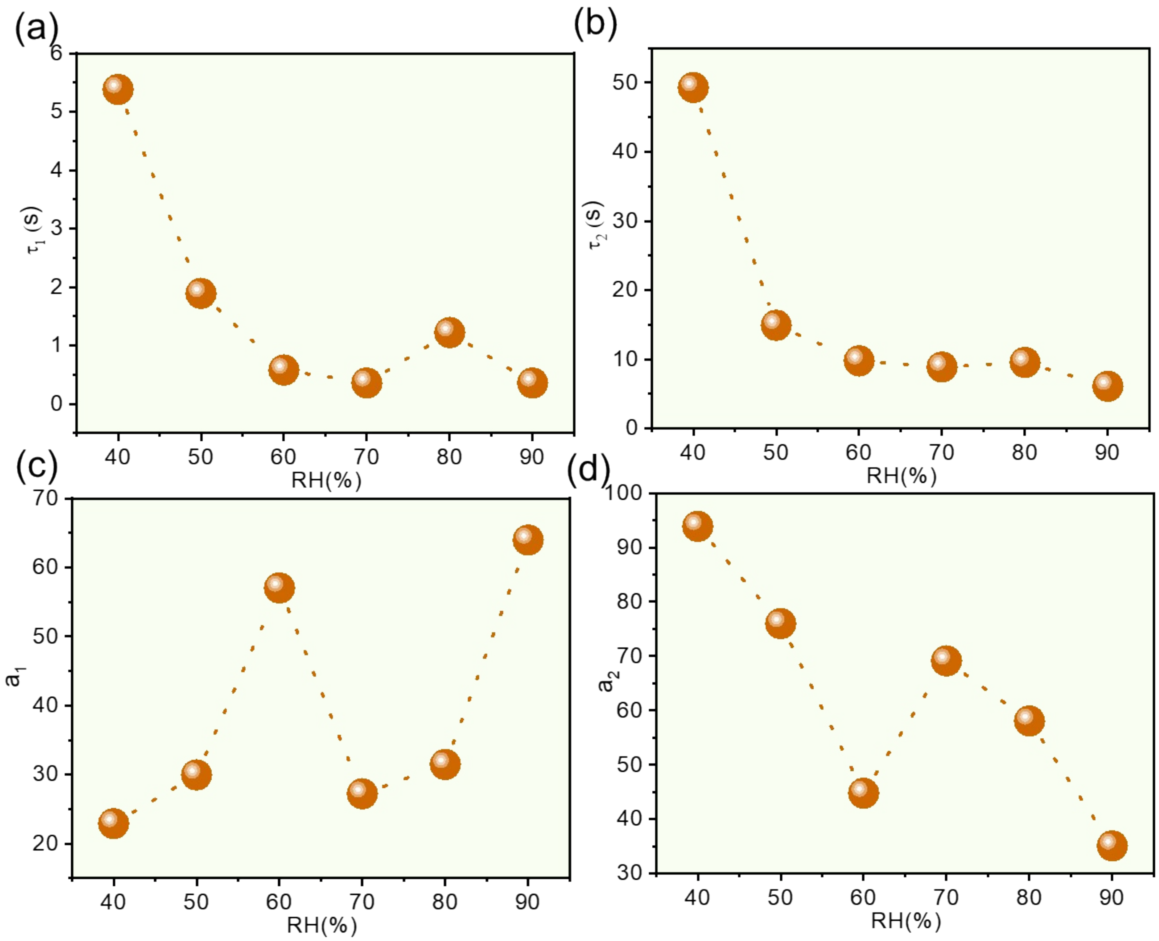

Figure S7 The variation of the parameters (a) τ_1 (b) τ_2 (c) a_1 and (d) a_2 with increasing RH for the decay after the application of 50 optical pulses.

Note S2

All the decay curves shown in Figure 2b are fitted with the double exponential function as shown below:

$$\frac{\Delta A}{\Delta A_{max}} = A_0 + a_1 e^{-t/\tau_1} + a_2 e^{-t/\tau_2}$$

Where,

$\Delta A = A_t - A_0$ with A_t being the current at time 't' and A_0 is the dark current

$\Delta A_{max} = A_{max} - A_0$ with A_{max} being the maximum current that is achieved during the optical exposure

a_1 and a_2 are the initial amplitudes of the fast and slow decay, respectively

τ_1 and τ_2 are the time constants for the fast and slow decay, respectively.

The τ_1 and τ_2 values alone indicates the rate of fast and slow decay. These values are decreasing with increase in RH showing that the decay becomes faster during both the processes with increase in RH. However, the consolidation parameter τ_2-τ_1 defines the temporal distinction between the fast and slow decay. With, τ_2-τ_1 being larger it can be said that the fast and slow decay processes are well-separated with slower decay starting much later to the faster one. Whereas, if τ_2-τ_1 is smaller, it indicates that both fast and slow processes overlap with each other with no clear distinction. This quantity has thus been used as a consolidation parameter where a larger τ_2-τ_1 suggest an effective consolidation with less interference between the decay processes and a smaller τ_2-τ_1 indicates a poorer consolidation due to increased interferences as the fast and slow processes overlap. a_1 and a_2 are the initial amplitudes of fast and slow decay. a_1 showing an approximately increasing trend with RH might indicate a larger contribution from the fast process with increased RH which further supports the poor consolidation at high RH. a_2 shows a decreasing trend with RH which again confirms that the slower decay is starting at a much later stage to the faster one at high RH. The parameters obtained from the equation thus proves that the faster decay dominates at high RH leading to poorer consolidation and the slower decay at low RH resulting in effective consolidation. In all the further studies, the consolidation parameter τ_2-τ_1 is considered alone for explaining the extent of consolidation as a_1 and a_2 follows a similar trend as explained here.

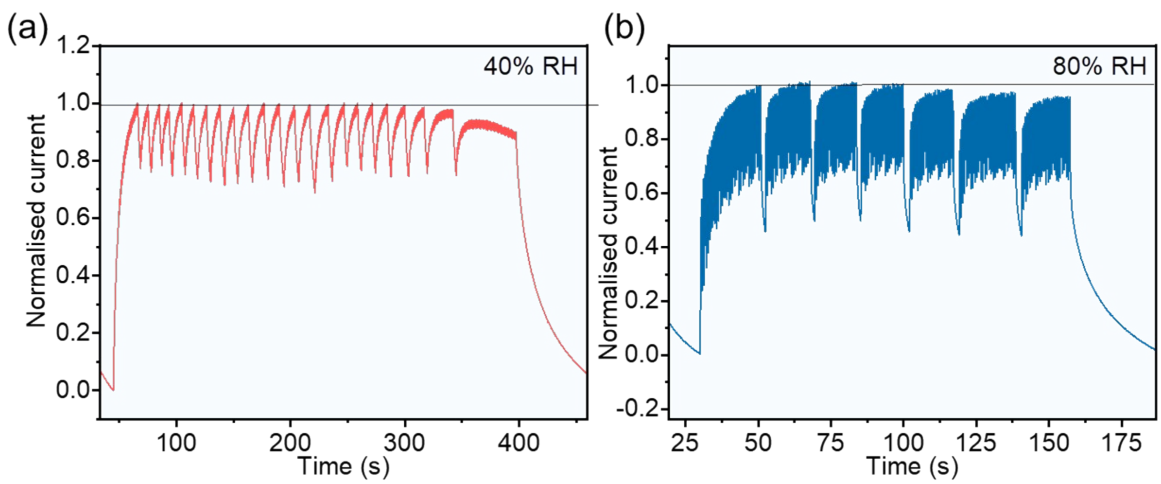

Figure S8 Experimental learning-forgetting-relearning curves at (a) 40% and (b) 80% RH.

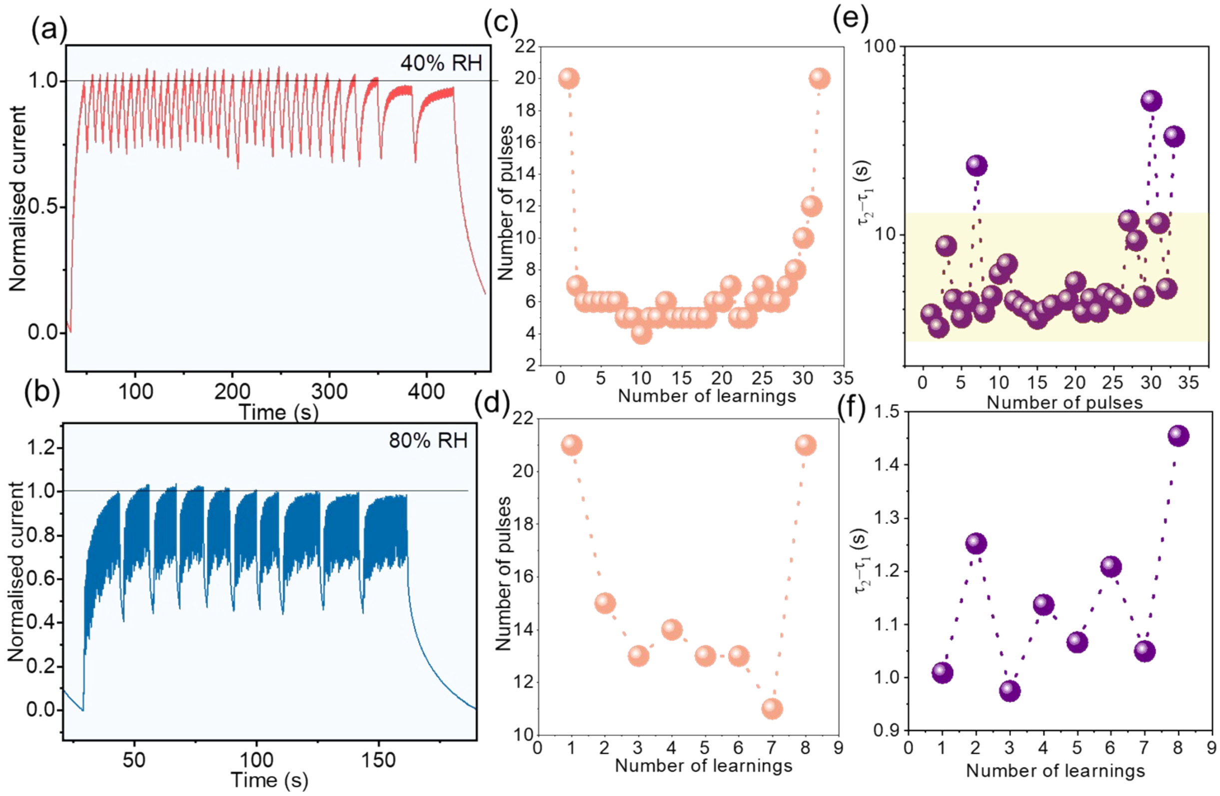

Figure S9 Learning-forgetting-relearning emulated at (a) 40% (normalized with respect to ~1.6 nA) and (b) 80% RH (normalized with respect to ~58.8 nA) with the initial learning performed with 20 pulses. Number of pulses required for consecutive learnings at (c) 40% and (d) 80% RH. The variation of τ_2-τ_1 (consolidation parameter) with the learning process at (e) 40% and (f) 80% RH.

Note S3

As explained in Figure 3, at 40% RH, the consolidation parameter (τ_2-τ_1) is almost the same during several learnings (Figure S9e) indicating faster consolidation due to lesser learning. However, at 80% RH, it is observed that τ_2-τ_1 slightly increases with learnings but not significantly as observed in Figure 3f which might be due to the lesser number of pulses (20 as opposed to 30 initial pulses in Figure 3) used for learning leading to faster consolidation.

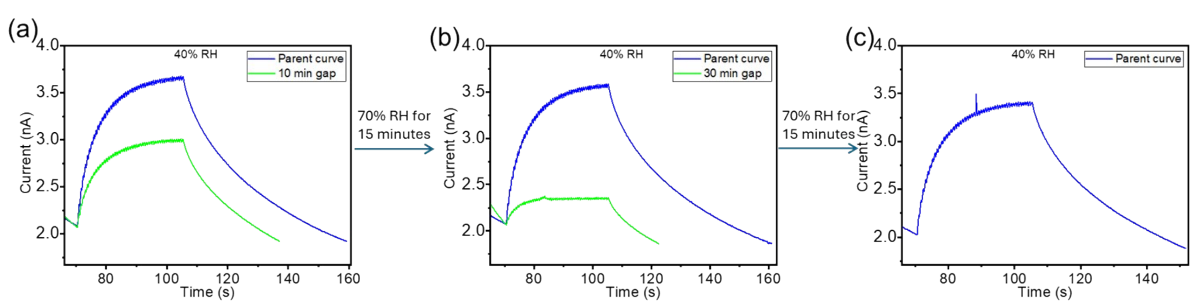

Figure S10 (a) Optical response at 40% RH for 50 pulses with the parent curve (blue) and the curve after 10 minutes time gap (green). (b) Recovery of the optical response (blue curve) after exposure to 70% RH for 15 minutes and the decrease in photoresponse with 30 minutes time gap (green curve). (c) Recovery of the photoresponse again after exposure to 70% RH for 15 minutes.

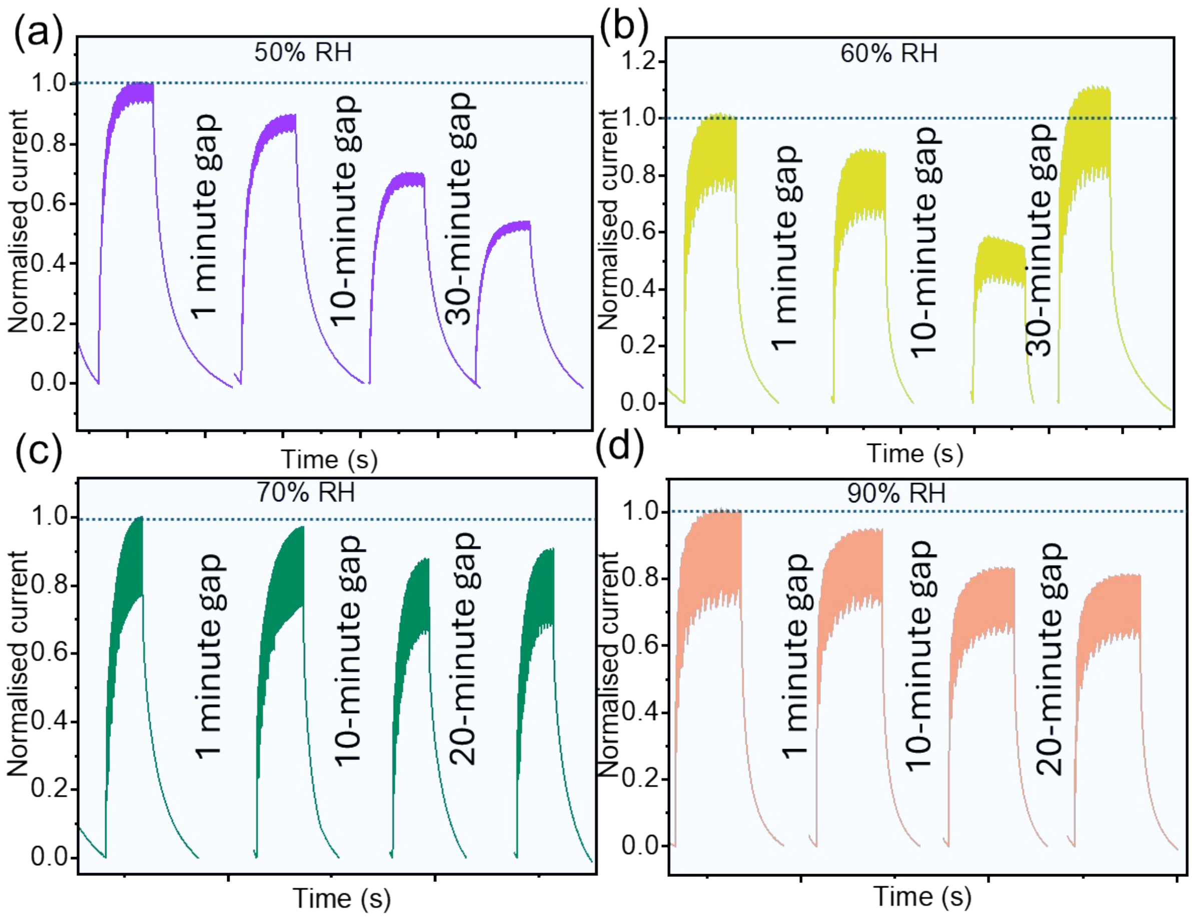

Figure S11 Photocurrent at (a) 50% (normalized with respect to ~10.9 nA), (b) 60% (normalized with respect to ~35.6 nA), (c) 70% (normalized with respect to ~91.2 nA) and (b) 90% RH (normalized with respect to ~188.2 nA) studied by varying the time gap.

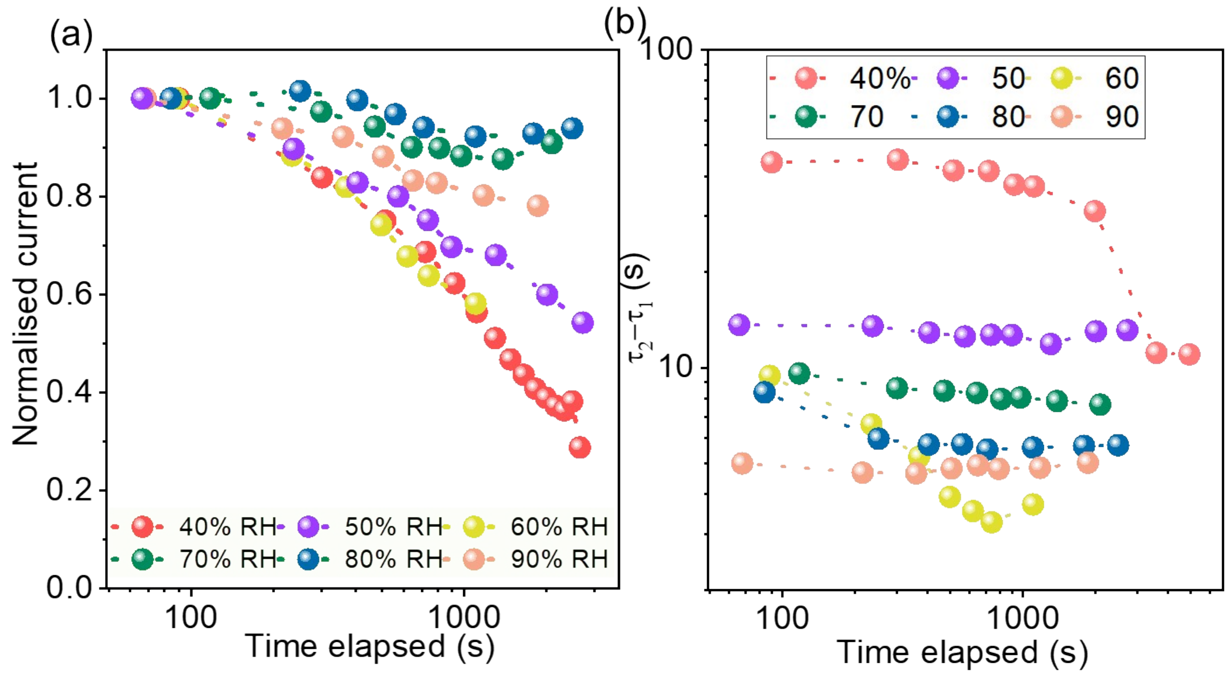

Figure S12 Variation in (a) current and (b) consolidation parameter τ_2-τ_1 with time at different RH.

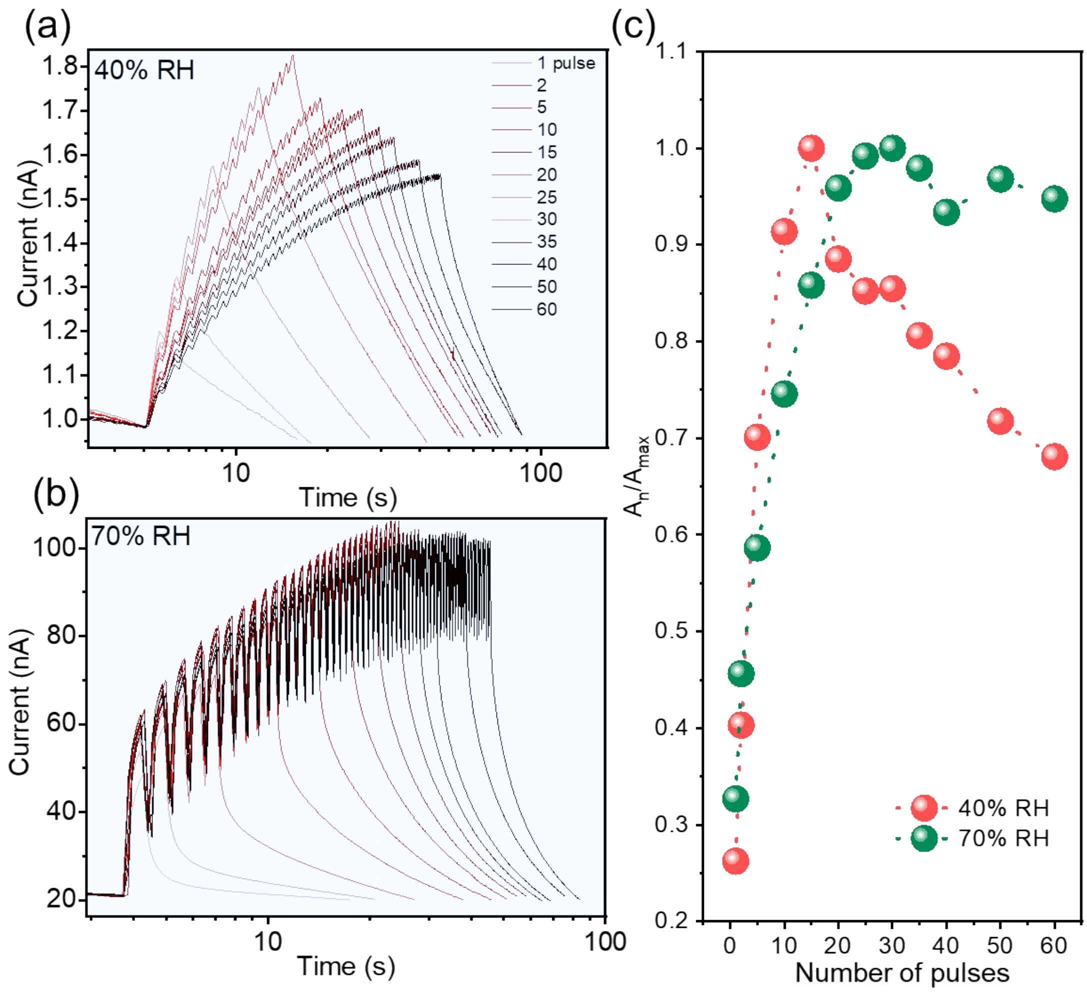

Figure S13 Photoresponse with increasing number of pulses at (a) 40% and (b) 70% RH. (c) Variation in photoresponse with the increase in the number of pulses at 40 and 70% RH.

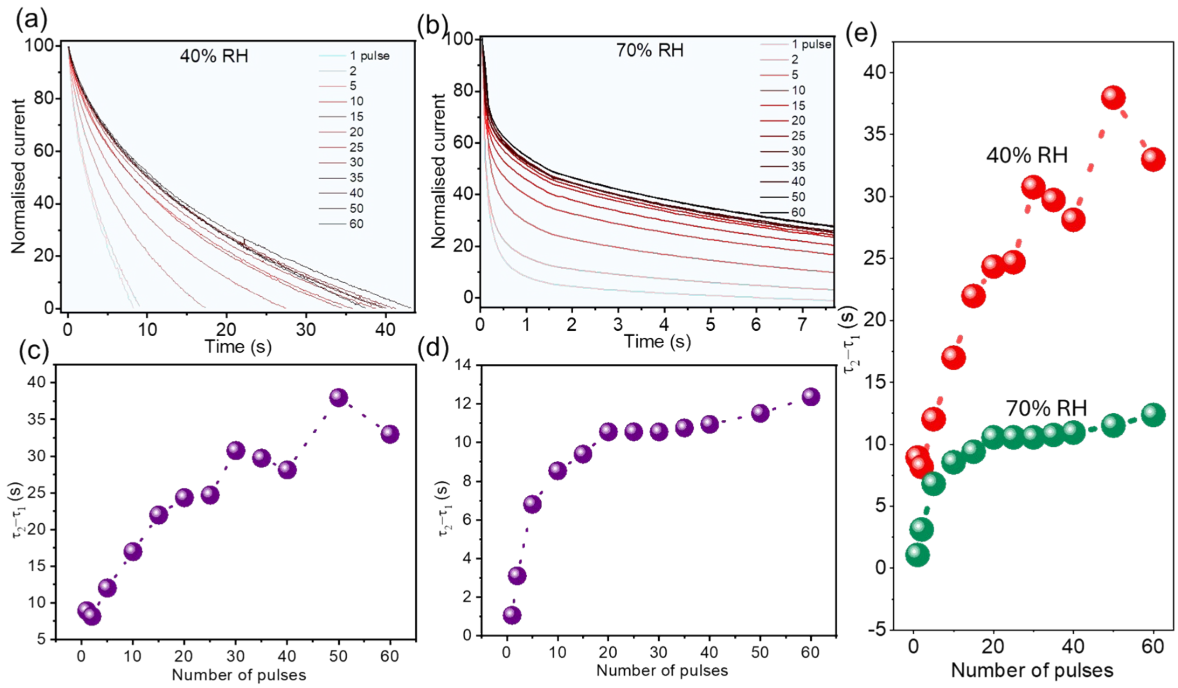

Figure S14 Decay curves with varying number of pulses at (a) 40% and (b) 70% RH. Variation in the consolidation parameter τ_2-τ_1 at (c) 40% and (d) 70% RH. (e) Comparison of variation in the consolidation parameter at 40 and 70% RH.

Note S4

Initially, if a lesser number of pulses are used for learning, fatigue does not occur immediately but progresses as the number of pulses increases (Figure S13a) at 40% RH (up to 10 pulses, the photocurrent gradually increases with the number of pulses after which it decreases) whereas the learning increases with the increase in the number of pulses at 70% RH (Figures S13b, 13c). Nonetheless, the consolidation parameter τ_2-τ_1 (Figure S14) increases with the increase in the number of pulses. However, it has to be noted that the decrement in the current response is only ~30% (Figure S13c) with 60 pulses at 40% RH which is similar to the photoresponse for the second set of pulses in Figure 4a (which apparently showed larger τ_2-τ_1). So, the gradual increase in the number of pulses outweighs the fatigue induced resulting in better consolidation. This again indicates that a greater number of optical exposures and increased electric field-induced stress results in faster fatigue at low RH but does not cause a lot of change at high RH.

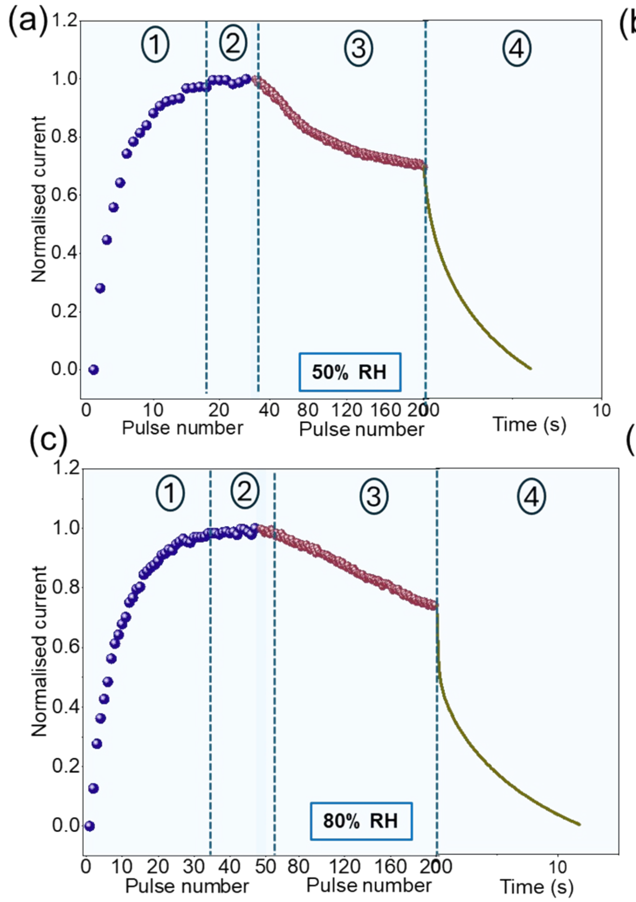

Figure S15 Learning profile exhibited at (a) 50% (normalized with respect to ~10.8 nA), (b) 60% (normalized with respect to ~16.6 nA), (c) 80% (normalized with respect to ~125.1 nA) and (b) 90% RH (normalized with respect to ~127.1 nA). The four stages of learning are 1-potentiation, 2-habituation, 3-depression, and 4-spontaneous forgetting.

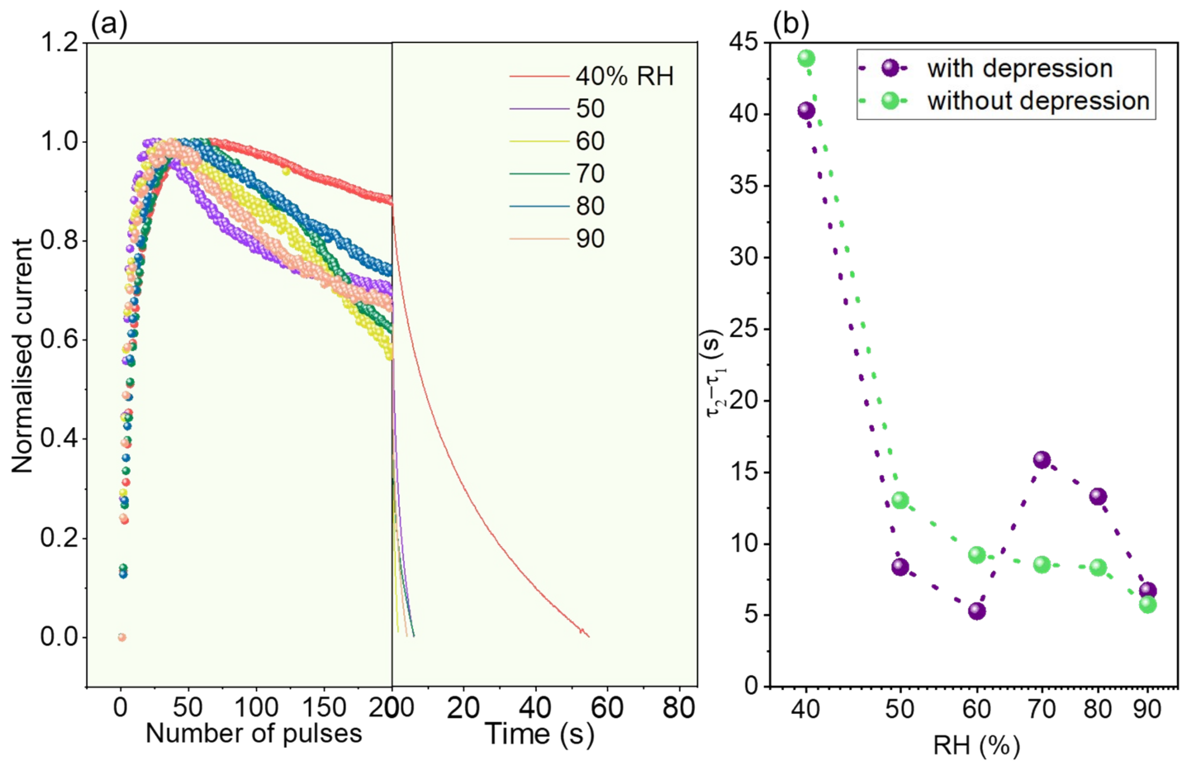

Figure S16 (a) Photocurrent and decay variation with RH during the application of 200 pulses. (b) Comparison of the consolidation parameter variation (τ_2 - τ_1) without and with depression behavior, as observed in Figures 2c and 5e, respectively.

Note S5

The equations used to obtain the non-linearity factor for potentiation and depression are;

$G_P = G_{min} + G_0(1 - e^{-\gamma_P N})$ for potentiation

$G_D = G_{max} - G_0(1 - e^{-\gamma_D(1 - N)}$ for depression

Where,

G_P and G_D represents the conductance during potentiation and depression, respectively

G_{min} and G_{max} are the minimum and the maximum conductance values

$G_0 = \dfrac{G_{max} - G_{min}}{1 - e^{-\gamma_P}}$ and $G_0 = \dfrac{G_{max} - G_{min}}{1 - e^{-\gamma_D}}$ in the case of potentiation and depression, respectively

γ_P and γ_D are the non-linearity factors for potentiation and depression, respectively which is 0 in the ideal case

It must be noted that the γ_P at all RHs are between 3 to 4.5. This indicates that the conductance saturates and reaches G_{max} with a small number of pulses.[32] This is due to the saturation in the number of photogenerated charge carriers. Further, γ_D is comparatively lower with the values ranging between -0.7 to 2. The $\gamma_D < 1$ when the depression curve is concave-down and $\gamma_D > 1$ when the curve is convex-up.[33]

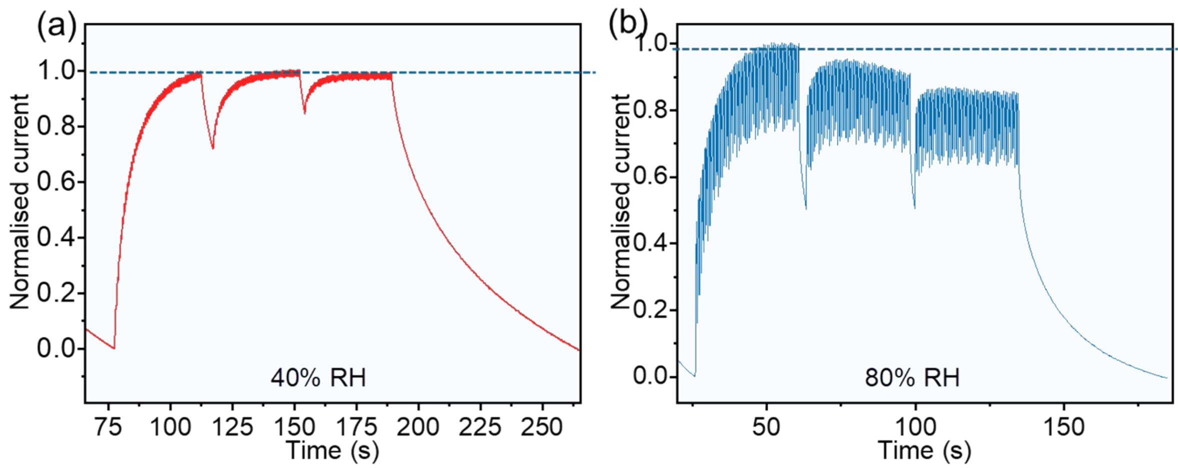

Figure S17 Photoresponse at (a) 40% (normalized with respect to ~2 nA) and (b) 80% RH (normalized with respect to ~90.4 nA) with the application of 50 optical pulses consecutively.

Note S6

Instead of 200 pulses, even if 50 pulses are applied continuously (Figure S17) with little time to decay, habituation and depression can be significantly observed at 80% RH and mildly at 40% RH with consolidation parameters being ~14 s and 46 s, respectively (quite similar to that obtained by applying 200 pulses continuously). Thus, if optical pulses are fed to the device with little to no time after the response has reached habituation will eventually lead to depression. Even though 40% RH is a less favorable environment, since the learning is poor, depression occurs at a slower rate but due to increased learning at high RH (a more favorable environment), depression is faster.

References

1 S.-N. L. Jae-Hyeok Oh, Jeong-Hyeon Kim, Hee-Jin Kim, Young-Hyeun Kim, Kyoung-Kook Kim, *Adv. Intell. Syst.*, 2023, **5**, 2300350.

2 and N. E.-A. Dayanand Kumar, Hanrui Li, Uttam Kumar Das, Abdul Momin Syed, *Adv. Mater.*, 2023, **35**, 2300446.

3 J. Liang, X. Yu, J. Qiu, M. Wang, C. Cheng, B. Huang, H. Zhang, R. Chen, W. Pei and H. Chen, *ACS Appl. Mater. Interfaces*, 2022, **15**, 9584–9592.

4 Y. Li, H. Sun, L. Yue, F. Yang, X. Dong, J. Chen, X. Zhang, J. Chen, Y. Zhao, K. Chen and Y. Li, *J. Phys. Chem. Lett.*, 2024, **15**, 8752–8758.

5 X. Liu, D. Wang, W. Chen, Y. Kang, S. Fang, Y. Luo, D. Luo, H. Yu, H. Zhang, K. Liang, L. Fu, B. S. Ooi, S. Liu and H. Sun, *Nat. Commun.* , 2024, **15**, 1–12.

6 X. Zhou, F. Hu, Q. Hou, J. Hu, Y. Wang and X. Chen, *Commun. Mater.*, 2024, **5**, 1–8.

7 J. Tang, Y. Q. Xiong, L. Y. Ye, Y. H. Li, W. J. Li and P. Yu, *ACS Appl. Mater. Interfaces*, 2024, **16**, 52692–52702.

8 F. Wu and T. Y. Tseng, *ACS Appl. Electron. Mater.*, 2024, **6**, 5212–5221.

9 A. H. Jaafar, S. K. S. Al Habsi, T. Braben, C. Venables, M. G. Francesconi, G. J. Stasiuk and N. T. Kemp, *ACS Appl. Mater. Interfaces*, 2024, **16**, 43816–43826.

10 C. Liu, Y. Ma, S. Sun, L. Zhu, L. Gao, J. Lei and T. Zi, *J. Phys. D. Appl. Phys.*, 2025, **58**, 025101.

11 Z. Weng, T. Ji, Y. Yu, Y. Fang, W. Lei, S. Shafie, N. Jindapetch and Z. Zhao, *ACS Appl. Nano Mater.*, 2024, **7**, 21018–21025.

12 X. Gao, T. Jiang, H. Li, J. Zhang, J. Huang, D. Ji and W. Hu, *Chem. Eng. J.*, 2024, **498**, 155237.

13 R. Yang, Y. Tian, L. Hu, S. Li, F. Wang, D. Hu, Q. Chen, X. Pi, J. Lu, F. Zhuge and Z. Ye, *Mater. Today Nano*, 2024, **26**, 100480.

14 J. H. Jun Wang, Ben Yang, Shilei Dai, Pu Guo, Yushan Gao, Li Li, Ziyi Guo, Junyao Zhang, Jianhua Zhang, *Adv. Mater. Technol.*, 2023, **8**, 2300449.

15 J. Liang, X. Yu, C. Cheng, B. Huang, Z. Wang and L. Huang, *J. Mater. Chem. C*, 2024, **12**, 14955–14963.

16 H. Yang, Y. Zhang, F. Hu, Z. Li, D. Wu and X. Chen, *ACS Appl. Mater. Interfaces*, 2024, **16**, 57804–57815.

17 Z. Wu, J. Lu, T. Shi, X. Zhao, X. Zhang, Y. Yang, F. Wu, Y. Li, Q. Liu and M. Liu, *Adv. Mater.*, 2020, **32**, 1–9.

18 X. Li, G. Li, Z. Zhang, W. Zhai, W. Zheng, L. Chen, L. Lin, X. Zhou, Z. Yan and J. Liu, *Appl. Phys. Lett.*, 2023, **122**, 183505.

19 R. Miyake, Z. Nagata, K. Adachi, Y. Hayashi, T. Tohei and A. Sakai, *ACS Appl. Electron. Mater.*, 2022, **4**, 2326–2336.

20 J. Hur, B. C. Jang, J. Park, D. Il Moon, H. Bae, J. Y. Park, G. H. Kim, S. B. Jeon, M. Seo, S. Kim, S. Y. Choi and Y. K. Choi, *Adv. Funct. Mater.*, 2018, **28**, 1–10.

21 T. Shi, J. F. Wu, Y. Liu, R. Yang and X. Guo, *Adv. Electron. Mater.*, 2017, **3**, 1–10.

22 X. Yang, Y. Fang, Z. Yu, Z. Wang, T. Zhang, M. Yin, M. Lin, Y. Yang, Y. Cai and R. Huang, *Nanoscale*, 2016, **8**, 18897–18904.

23 B. Zhao, M. Xiao, D. Shen and Y. N. Zhou, *Nanotechnology*, 2020, **31**, 125201.

24 R. Jiang, P. Ma, Z. Han and X. Du, *Sci. Rep.*, 2017, **7**, 1–8.

25 L. Yang, D. Lin, M. Qi, X. Xiu, H. Dong and H. Wang, *Phys. Status Solidi - Rapid Res. Lett.*, 2021, **2100255**, 1–8.

26 Z. Wen, W. Sheng, L. Ai, Y. Li, X. Li and H. Xiao, *J. Mater. Sci. Technol.*, 2023, **160**, 204–213.

27 U. Mogera, A. A. Sagade, S. J. George and G. U. Kulkarni, *Sci. Rep.*, 2014, **4**, 1–9.

28 U. Mogera, M. Gedda, S. J. George and G. U. Kulkarni, *ACS Appl. Mater. Interfaces*, 2017, **9**, 32065–32070.

29 S. Kundu, U. Mogera, S. J. George and G. U. Kulkarni, *Nano Energy*, 2019, **61**, 259–266.

30 S. Kundu, S. J. George and G. U. Kulkarni, *ACS Appl. Mater. Interfaces*, 2023, **15**, 19270–19278.

31 T. S. Rao, S. Kundu, B. Bannur, S. J. George and G. U. Kulkarni, *Nanoscale*, 2023, **15**, 7450–7459.

32 J. Kang, T. Kim, S. Hu, J. Kim, J. Y. Kwak, J. Park, J. K. Park, I. Kim, S. Lee, S. Kim and Y. Jeong, *Nat. Commun.*, 2022, **13**, 4040.

33 J. H. Baek, K. J. Kwak, S. J. Kim, J. Kim, J. Y. Kim, I. H. Im, S. Lee, K. Kang and H. W. Jang, *Nano-Micro Lett.*, 2023, **15**, 1–18.